Mechanically Attrited Silicon for High Refractive Index Nanocomposites

Fotios Papadimitrakopoulos,* Peter Wisniecki, and Dorab E. Bhagwagar†

Department of Chemistry, Polymer Science Program, Institute of Materials Science, University of Connecticut, Storrs, Connecticut 06269

Received April 30, 1997. Revised Manuscript Received July 7, 1997⊗

High-energy milling provides an effective and environmentally conscious method for nanosizing silicon. Colloidal suspensions of nanosized silicon are presently demonstrated and utilized for the fabrication of high refractive index nanocomposites. Si nanoparticles with average sizes of 20−40 nm and size distributions of about 25% have been separated from milled powder via sonication and centrifugation. These nanoparticles were analyzed using transmission electron microscopy, dynamic light scattering, X-ray diffraction and UV−vis/FTIR spectroscopy. Formation of stable colloids is in part attributed to a thin surface-oxide layer. The decrease in the average particle size causes a blue shift in their absorption spectrum, thus increasing transparency in the red part of the visible region. These Si nanoparticles were used to fabricate high refractive index nanocomposites, with refractive indexes up to 3.2, when dispersed in gelatin.

Introduction

Nanosized materials have generated enormous interest during the past few years.[1−3] One of the means of harvesting their specialized properties, in products of defined size and shape, is by incorporating them into polymeric matrixes.[4,5] Polymer nanocomposites that exhibit enhanced mechanical,[6,7] magnetic,[8,9] optical,[7,10,11] electrical,[8,12,13] optoelectronic,[14−16] and electrooptic[8,11,17] properties have been widely reported.

In recent years nanoparticles have been used toward the fabrication of high refractive index nanocomposites.[18−20] Such materials could potentially bridge the large refractive index gap between organic/inorganic interfaces and help improve the optical-coupling efficiencies in photonic devices.[21] For example, the refractive indexes of polymers vary between 1.3 and 1.7, while those of inorganic semiconductors vary between 2 and 5.[22] Some specialty polymers can exhibit a refractive index greater than 2, such as poly(thiophene) with $n = 2.12$,[23] although this is strongly coupled to optical absorbance in the visible region. Inorganic high-bandgap materials, such as TiO_2, could reach up to refractive indexes of 2.9 in their crystalline state, but above this limit it is necessary to consider composites of inorganic semiconductors such as those presented in Table 1.[22]

Table 1. Refractive Indexes and Absorption Coefficients at Three Different Wavelengths in the Visible Range for Some of the Ultrahigh Refractive Index Semiconductor Inorganics

	refractive index (n)			absorption coefficient (k)		
material	4000 Å	5000 Å	6200 Å	4000 Å	5000 Å	6200 Å
crystalline Si	5.57	4.298	3.906	0.387	0.073	0.022
amorphous Si	4.38	4.47	4.23	2.02	0.992	0.461
Ge	4.141	4.34	5.588	2.215	2.384	0.933
GaP	4.196	3.59	3.325	0.275	2.5 × 10-3	2.8 × 10-7
InP	4.415	3.818	3.549	1.735	0.511	0.317
PbS	3.62	4.35	4.194	2.015	2.238	1.773

High refractive index nanocomposites of PbS nanoparticles in gelatin or poly(ethylene oxide) have been thoroughly investigated by Suter et al.[18−20] Their studies indicate that both PbS particle size and loading

* To whom correspondence should be addressed.
† Present address, Dow Corning Corp., Adhesives Dept. M/S C40A00, Midland, MI 48686.
⊗ Abstract published in *Advance ACS Abstracts,* October 1, 1997.

(1) Klabunde, K. J. *Free Atoms, Clusters, and Nanoscale Particles*; Academic Press: San Diego, 1994.
(2) Moser, W. R. *Advanced catalysts and nanostructured materials: modern synthetic methods*; Academic Press: San Diego, 1996.
(3) Hoch, H. C.; Jelinski, L. W.; Craighead, H. G. *Nanofabrication and biosystems: integrating materials science, engineering and biology*; Cambridge University Press: Cambridge, 1996.
(4) Mark, J. E.; Lee, C. Y.-C.; Bianconi, P. A. *Hybrid organic−inorganic composites*; American Chemical Society: Washington, DC, 1995; Vol. 585.
(5) Komarneni, S.; Parker, J. C.; Thomas, G. J. *Nanophase and nanocomposite materials*; Materials Research Society: Pittsburgh, PA, 1993.
(6) Otooni, M. A. *Grain size and mechanical properties: fundamentals and applications*; Materials Research Society: Pittsburgh, 1995; Vol. 362.
(7) Schmidt, H. K. *Macromol. Symp.* **1996**, *101*, 333.
(8) Clement, R. In *Hybrid Organic Inorganic Composites*; Mark, J. E., Ed.; American Chemical Society: Washington, DC, 1995; Vol. 585; p 29.
(9) Hess, P. H.; Parker, P. H. J. *J. Appl. Polym. Sci.* **1966**, *10*, 1915.
(10) Ogawa, T.; Kanemitsu, Y. *Optical properties of low-dimensional materials*; World Scientific: River Edge, NJ, 1995.
(11) Levy, D.; Esquivias, L. *Adv. Mater.* **1995**, *7*, 120.
(12) Kanatzidis, M. G.; Wu, C. *J. Am. Chem. Soc.* **1989**, *111*, 4139.
(13) Kanatzidis, M. G.; Wu, C.; Marcy, H. O.; DeGroot, D. C.; Kannewurf, C. R. *Chem. Mater.* **1990**, *2*, 222.
(14) Henneberger, F.; Schmitt-Rink, S.; Gobel, E. O. *Optics of semiconductor nanostructures*; Akademie Verlag: Berlin, Germany, 1993.
(15) Alivistatos, A. P. *J. Phys. Chem.* **1996**, *100*, 13226.
(16) Brus, L. *J. Phys. Chem.* **1994**, *98*, 3575.
(17) Wang, Y.; Suna, A.; Mahler, W. *Mater. Res. Soc. Symp. Proc.* **1988**, *109*, 187.
(18) Weibel, M.; Caseri, W.; Suter, U. W.; Kiess, H.; Wehrli, E. *Polym. Adv. Technol.* **1991**, *2*, 75.
(19) Zimmermann, L.; Weibel, M.; Caseri, W.; Suter, U. W. *J. Mater. Res.* **1993**, *8*, 1742.
(20) Kyprianidou-Leodidou, T.; Caseri, W.; Suter, U. W. *J. Phys. Chem.* **1994**, *98*, 8992.
(21) Kitai, A. H. *Solid State Luminescence*; Chapman & Hall: London, 1993.
(22) Palik, E. D. *Handbook of Optical Constants of Solids*; Academic Press: Orlando, 1985.
(23) Sugiyama, T.; Wada, T.; Sasabe, H. *Synth. Met.* **1989**, *28*, C323.

S0897-4756(97)00278-0 CCC: $14.00

Table 2. Volume and Weight Fraction of Inorganic Phase Necessary to Produce Gelatin-Based Nanocomposites with Refractive Indexes of 2.5 at Three Different Wavelengths in the Visible Spectrum[22]

	weight fraction			volume fraction		
material	4000 Å	5000 Å	6200 Å	4000 Å	5000 Å	6200 Å
crystalline Si	0.35	0.48	0.54	0.24	0.35	0.41
amorphous Si	0.47	0.46	0.49	0.34	0.33	0.36
Ge	0.7	0.67	0.55	0.37	0.34	0.24
GaP	0.64	0.73	0.78	0.37	0.47	0.54
InP	0.62	0.72	0.77	0.33	0.42	0.48
PbS	0.83	0.74	0.76	0.47	0.34	0.36

influence the overall refractive index of the nanocomposite. Very small particles show reduced refractive index as compared to that of particles with diameter equal or greater than 25 nm which approach the refractive index of bulk PbS.[20] The absorption coefficient of PbS nanoparticles showed nanoparticle-size behavior similar to that of refractive index. On the basis of on their experimental data Suter et al. have shown that the overall refractive index of the nanocomposite n is to the first approximation proportional to the volume fractions v_i and refractive indexes n_i of its components respectively ($n = n_1v_1 + n_2v_2$ for a two-component system).[20]

The technological challenges to achieve high refractive index inorganic−organic nanocomposites ($n > 2.5$) of increased transparency require the use of high refractive index nanoparticles with low absorption coefficient in the visible range and diameter between 20 and 40 nm (well below one-tenth of the wavelength of light (400−800 nm) in order to suppress Rayleigh scattering). For the same reasons, agglomerates and large sized scatterers, such as voids, should be scrupulously excluded.

On the basis of the absorption coefficient of ultrahigh refractive index inorganics listed in Table 1, PbS and Ge are unlikely candidates. GaP, on the other hand, appears to be the material of choice with second to best crystalline Si.[22] While the refractive indexes are additive on a volume fraction basis, the specific gravity of the inorganic phase determines its weight fraction in the composite. Silicon is the least dense of the group in Table 1 with 2.32 g/cm^3, followed by GaP with 4.14 g/cm^3, InP with 4.84 g/cm^3, Ge = 5.32 g/cm^3, and PbS with 7.50 g/cm^3. Table 2 shows the volume and weight fraction of the inorganic phase necessary to achieve a nanocomposite with refractive index of 2.5 in gelatin at three different wavelengths. This calculation was based on the volume fraction formula, used by Suter et al.,[20] even though tge effective medium approximation (EMA) has been shown to give a better representation of the composite refractive index.[24,25] It quickly becomes apparent that Si offers the best-case scenario, by both volume and weight fraction, to achieve such a nanocomposite allowing the inorganic phase to be adequately dispersed, to minimize scattering due to particle aggregation. In addition, the inherently low density and cost of such composites could potentially appeal to the silicon-based industry resulting in potential novel applications.

Several preparation techniques for silicon nanoparticles have been reported such as chemical-vapor pyrolysis or deposition,[26−31] sputtering,[32−34] gas evaporation,[35] anodic etching,[36−40] and high-energy milling.[41] Electrochemical etching followed by electropolishing have been used to prepare porous silicon films of increased transparency with the index of refraction n calculated to be 2 in the IR.[42] Ultimately, high-energy milling was chosen based on its environmental friendliness, low cost, and relative ease of nanoparticle separation. However this technique introduces some limitation with respect to chemical purity and partial amorphization (which results in increased absorption, see Table 1) as a result of milling. Chemical etching could potentially overcome these shortcomings and allow these nanoparticles to be used in semiconductor-based applications. This paper describes the initial results on separation and characterization of these nanoparticles which were later used to fabricate gelatin-based high refractive index nanocomposites with values as high as 3.2.

Experimental Section

Milling: Polycrystalline Si powder of 99.5% nominal purity and 325 mesh size was procured from Alfa Aesar. Milling was performed in a round-ended hardened steel vial with two $^1/_2$ in. and four $^1/_4$ in. hardened steel balls provided by Spex Sample Prep. Si powder (2.0 g) was loaded into the steel vial while inside a glovebox to maintain an inert nitrogen atmosphere during milling. A high-energy Spex 8000 shaker mill was used for the ball milling. After milling, the steel vial was unloaded in a glovebox and the nanomilled silicon was stored in inert atmosphere.

Preparation of colloidal silicon: Nanomilled Si powder (200 mg) was placed in a polypropylene container and sonicated overnight in 30 mL of ethanol (200-proof) with the help of a Fisher Scientific FS9 ultrasonic cleaning bath to produce a black suspension. Colloidal Si nanoparticles were separated by centrifugation at 3000 rpm for 90 min. in a Sorvall SuperSpeed RC2-B centrifuge. The yellow-orange supernatant was carefully removed with a glass pipet and stored away from direct sunlight.[26] This very weakly opalescent, colloidal suspension was found to be extremely stable for many months. For nanoparticles between 20 and 40 nm, the yield is about 4%.

Characterization techniques: Transmission electron micrographs of Si nanoparticles were obtained on a Phillips

(24) Tompkins, H. G. *A User's Guide to Ellipsometry*; Academic Press: Boston, 1993.
(25) Aspnes, D. E. *Thin Solid Films* **1992**, *89*, 249.
(26) Fojtik, A.; Weller, H.; Fiechter, S.; Henglein, A. *Chem. Phys. Lett.* **1987**, *134*, 477.
(27) Littau, K. A.; Szajowski, P. J.; Mullen, A. J.; Kortan, A. R.; Brus, L. E. *J. Phys. Chem.* **1993**, *97*, 1224.
(28) Takagi, H.; Ogawa, H.; Yamazaki, Y.; Ishizaki, A.; Nakagiri, T. *Appl. Phys. Lett.* **1990**, *56*, 2379.
(29) Rüchschloss, M.; Ambacher, O.; Veprek, S. *J. Lumin.* **1993**, *57*, 1.
(30) Zang, D.; Kolbas, R. M.; Milewski, P. D.; Lichtenwalner, D. J.; Kingon, A. I.; Zavada, J. M. *Appl. Phys. Lett.* **1994**, *65*, 2684.
(31) Nakajima, A.; Sugita, Y.; Kawamura, K.; Tomita, H.; Yokoyama, N. *J. Appl. Phys.* **1996**, *80*, 4006.
(32) Furukawa, S.; Niyasato, T. *Phys. Rev. B* **1988**, *38*, 5726.
(33) Osaka, Y.; Tsunetomo, K.; Toyomura, F.; Myoren, H.; Kohno, K. *Jpn. J. Appl. Phys.* **1992**, *31*, L365.
(34) Sun, Y.; Nishitani, R.; Miyasato, T. *Jpn. J. Appl. Phys.* **1994**, *33*, L1645.
(35) Morisaki, H.; Ping, F. W.; Ono, H.; Yazawa, K. *J. Appl. Phys.* **1991**, *70*, 1869.
(36) Canham, L. T. *Appl. Phys. Lett.* **1990**, *57*, 1046.
(37) Lehmann, V.; Gösele, U. *Appl. Phys. Lett.* **1991**, *58*, 856.
(38) Nakajima, A.; Itakura, T.; Watanabe, S.; Nakayama, N. *Appl. Phys. Lett.* **1992**, *61*, 46.
(39) Heinrich, J. L.; Curtis, C. L.; Credo, G. M.; Kavanagh, K. L.; Sailor, M. J. *Science* **1992**, *255*, 66.
(40) Bley, R. A.; Kauzlarich, S. M.; Davis, J. E.; Lee, H. W. H. *Chem. Mater.* **1996**, *8*, 1881.
(41) Shen, T. D.; Koch, C. C.; McCormick, T. L.; Nemanich, R. J.; Huang, J. Y.; Huang, J. B. *J. Mater. Res.* **1995**, *10*, 139.
(42) Behren, J. v.; Tsybeskov, L.; Fauchet, P. M. *Appl. Phys. Lett.* **1995**, *66*, 1662.

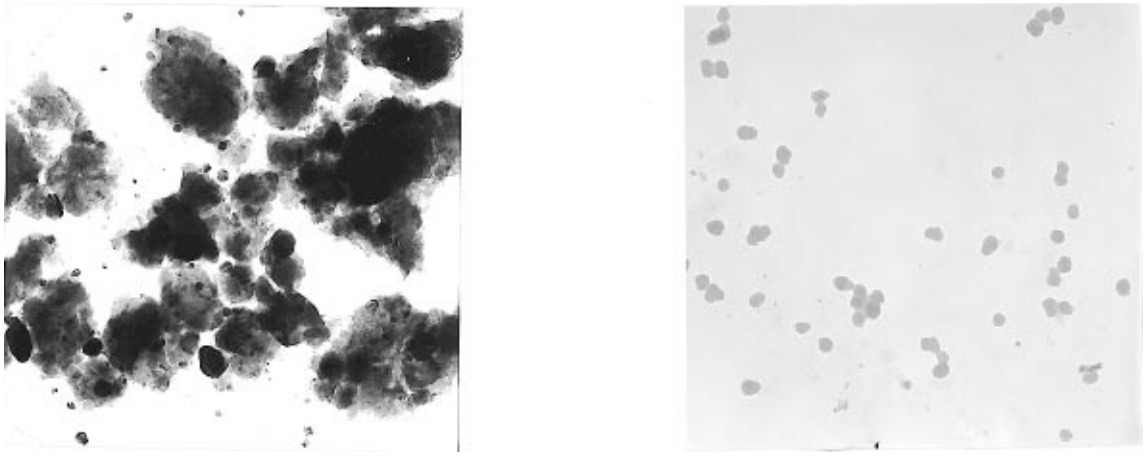

Figure 1. Bright-field transmission electron micrographs of Si, (A) as-milled, and (B) after separation by centrifugation.

EM 300 TEM operating at 80 kV acceleration, by casting a drop of a dilute suspension on carbon-coated copper grids and allowing the solvent (ethanol) to slowly evaporate.

Dynamic light scattering (DLS) was utilized to determine the mean particle size and distribution in dilute solutions with the help of a Nicomp 370 submicron particle sizer from Particle Sizing Systems Inc. A Nicomp size-distribution analysis was used that is based on a nonlinear least-squares analysis fitting of the inverse Laplace transform of the autocorrelation function.[43]

X-ray diffraction (XRD) was performed on a Norelco/Phillips diffractometer using Cu Kα radiation (λ = 1.5418 Å). The colloidal silicon was concentrated and casted on a glass slide allowing the ethanol to evaporate prior measuring its XRD spectrum, followed by subtraction of the substrate background.

UV−vis spectra were recorded on a Perkin-Elmer Lambda 3840 array spectrophotometer. Colloidal Si suspension concentrations were determined gravimetrically by slow evaporation of the ethanol in a stream of N_2 gas, followed by vacuum-drying.

Infrared (IR) spectroscopic data were obtained from a Nicolet 60-SX using a TeGeSe detector at 4 cm^{-1} resolution. Thin films of Si nanoparticles were deposited on KBr disks by a slow evaporation of ethanol in a stream of N_2 gas and dried in vacuum at around 70 °C. A minimum of 32 scans were signal averaged. The FTIR spectra of KBr disk was included into the spectrometer's background to ensure minimum signal contribution from the silicon substrate.

Preparation and analysis of silicon−gelatin nanocomposites: Gelatin polymer (Eastman Kodak) was solubilized in water and then the colloidal dispersion of Si in ethanol was added to result in ca. 50/50 w/w Si/gelatin mixture. This mixture was then concentrated by bubbling N_2 to increase its viscosity and it was then spin-coated at 750−1200 rpm on precleaned Si wafers followed by a 4 h vacuum annealing at 150 °C to facilitate film densification. Refractive indexes were measured on a J. A. Woollam Co. Variable-angle spectroscopic ellipsometer (VASE). Data were collected at wavelengths between 4000 and 10 000 Å with a 100 Å interval and at angles between 65° and 80°.

Results and Discussion

Preparation and characterization of colloidal silicon: The profound technological importance of the silicon-based industry has stimulated considerable investigation into attaining well-controlled nanosized Si.[26−41] Recently, Shen et al.[41] have reported the use of high-energy milling for nanosizing silicon in order to attain crystal grain sizes ranging from 3 to 20 nm. This has prompted us to employ this technique in order to produce nanosized Si, in large quantities, for the fabrication of high refractive index nanocomposites. Dispersing the freshly milled Si powder into solvents such as ethanol, water, and tetrahydrofuran (THF) has resulted in black suspensions that quickly flocculate to leave a clear supernatant. Mild sonication has resulted in similar suspensions that require considerably longer time to settle down. Figure 1a indicates that high-energy nanomilling yields particles with very broad size distributions (3−500 nm), clearly unsuitable for use in photonic applications.

Significant effort was put into the extraction of Si nanoparticles with well-defined average size (20−40 nm) and size distributions less than 20−30%. Several different methods were employed to achieve separation including filtration and centrifugation. A series of trials was performed and parameters such as exposure to oxygen and sonication time and temperature were proven crucial. The formation of an ultrathin silicon oxide that will be discussed later on in this paper appeared to be instrumental in stabilizing nanosilicon colloids.[26,27,31,40] Filtration of sonicated suspensions proved to be a less effective technique for separation of colloidal nanosilicon, highly likely due to the fact that small particles are attracted and halted during percolation through larger agglomerates. On the other hand, centrifugation quickly separates the large agglomerates from nanosilicon leaving a bright orange, lightly opalescent supernatant of colloidal Si. Optimization of sonication temperature (ca. 10 °C) and centrifugation time and speed has yielded colloidal Si with the desired average size and size distribution (see Figure 1B). In contrast to the black suspensions formed by the as-milled powder, the separated nanoparticles form stable colloids (for over 6 months).

The average size of these nanoparticles, as determined by TEM was corroborated by size distribution analysis obtained by dynamic light scattering (DLS) shown in Figure 2. The majority of nanoparticles lies between 20 and 30 nm (see Figure 1B). The correlation function obtained by DLS clearly does not obey Gaussian statistics. An alternative fitting procedure (Nicomp) developed especially for lightly agglomerated colloids (less than 1% agglomeration) has shown a near perfect fit based on a bimodal distribution shown in Figure 2.

(43) Nicoli, D. F.; McKenzie, D. C.; Wu, J. *Am. Lab.* **1991**,

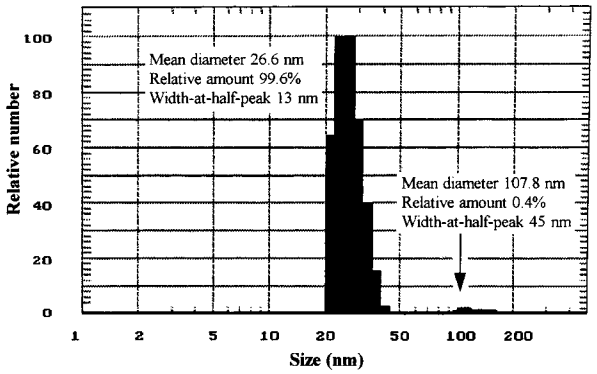

Figure 2. Number average particle size distribution obtained by dynamic light scattering from colloidal Si samples.

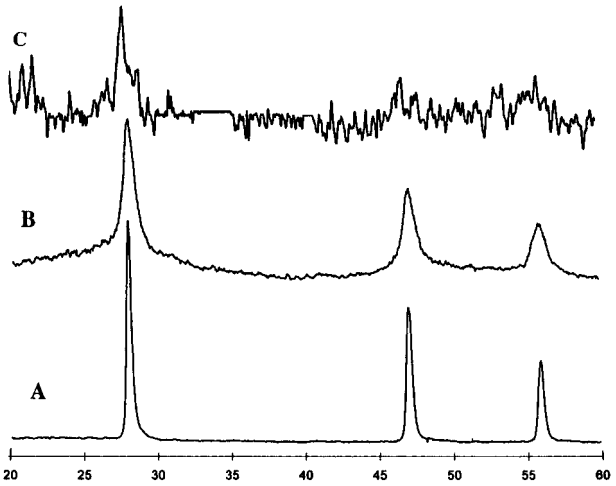

Figure 3. Radial X-ray diffraction profiles of (A) bulk Si, (B) as-milled sample Si, and (C) Si after separation by centrifugation.

The small fraction of particles in the range between 100 and 150 nm size is present in all colloidal nanosilicon samples, even at very dilute concentrations. On the basis of the fact that microfiltration through 100 nm Nylon as well as Teflon filters has failed to remove these agglomerates, it is believed that they originate from a dynamic agglomeration−deagglomeration process slow enough to be measured by DLS. These agglomerates might look like those present in Figure 1B although considerable caution has to be exercised based on the markedly different nature of sample preparation (liquid vs solid).

The X-ray diffraction (XRD) profiles for bulk silicon, as-milled powder (before separation) and separated nanoparticles are presented in Figure 3. Line broadening is clearly the biggest difference between bulk silicon and as milled sample (Figure 3A,B respectively). This is in agreement with the thorough investigation of Shen et al.,[41] on the high-energy ball milling of Si, where nanocrystalline grains of Si ranging from 3 to 20 nm were obtained, based on high-resolution TEM and XRD line broadening analysis.[41] A combination of pressure-induced amorphization and crystallite-refinement-induced amorphization was proposed to be responsible for this thermodynamically unfavorable process. The authors also verified that the partial amorphous (ca. 15%) character of the milled Si powder was distributed heterogeneously among the nanocrystalline portions while isolated nanocrystals were surrounded by a layer of amorphous silicon, surprisingly enough not oxidized

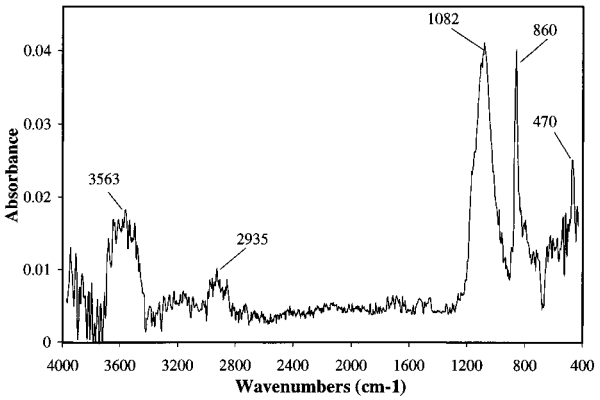

Figure 4. FT-IR transmission spectrum of colloidal silicon on KBr crystal.

by the adsorbed oxygen.[41] The XRD profile of the isolated nanosilicon in Figure 3C, although attained with significantly lower signal-to-noise ratio due to instrumentation shortcomings, resembles that of as-milled powder with marginally increased line-broadening. On the basis of the work of Shen et al.,[41] and the work presented below, it is currently believed that these nanoparticles consist of nanocrystalline Si interior with an amorphous Si exterior, partially coated with surface oxide which assists formation of colloidal suspensions in polar solvents.[26,27,40]

FTIR spectroscopy was shown to be an effective technique for the characterization of the surface of Si nanoparticles.[27,40,41,44] Figure 4 illustrates the transmission FTIR spectrum of these nanoparticles as casted on a KBr crystal. These results suggest that their surface is covered with a layer of oxide. The pronounced absorptions at 1082 and 860 cm^{-1} correspond to Si−O−Si and Si−O−H stretching, respectively. The 470 cm^{-1} absorbance corresponds to Si−O−Si rocking or bending vibrations.[44] Another indication of hydroxyl functionalities arise from the broad absorption at 3563 cm^{-1} from O−H stretch. The contribution of adsorbed moisture or ethanol to the 3563 cm^{-1} peak was carefully minimized by vacuum-drying at 100 °C. The presence of a weak absorption around 2900 cm^{-1} (aliphatic C−H stretch) has been attributed to chemisorbed hydrocarbons,[40] although the presence of Si−O−CH_2CH_3 could not be inferred due to pronounced Si−O−Si stretching present in roughly the same region as Si−O−Et stretching.

The amount of Si−O−Si which coats the surface of these nanosilicon particles seems to slowly accumulate with increasing sonication time in the presence of air and room light.[26] This gradually increases the polarity of nanoparticle surface and promotes solvation in polar solvent. When this is utilized in sequence with continuous extraction of the supernatant colloid after centrifugation, relatively narrow dispersed nanosilicon fractions with increasing mean-size can be obtained. Partial coverage of the nanosilicon surface with its oxide is presently believed to control the flotation of these particles in ethanol. Smaller particles require less oxidation to get suspended versus the larger ones that flocculate in large aggregates. Transmission FTIR spectroscopy of nanosilicon films with constant optical

(44) Feng, Z. C.; Tsu, R. *Porous Silicon*; World Scientific: River Edge, NJ, 1994.

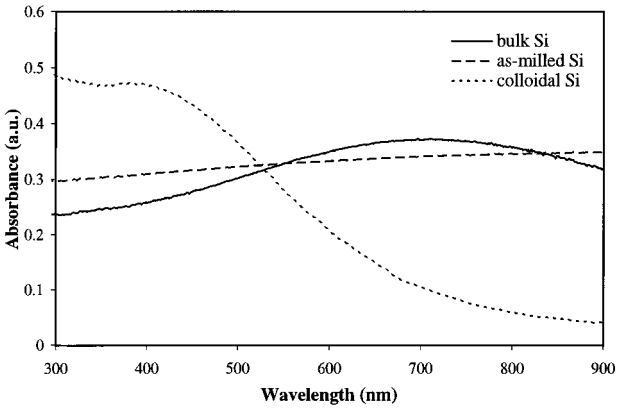

Figure 5. UV−vis absorbance spectra of different Si samples.

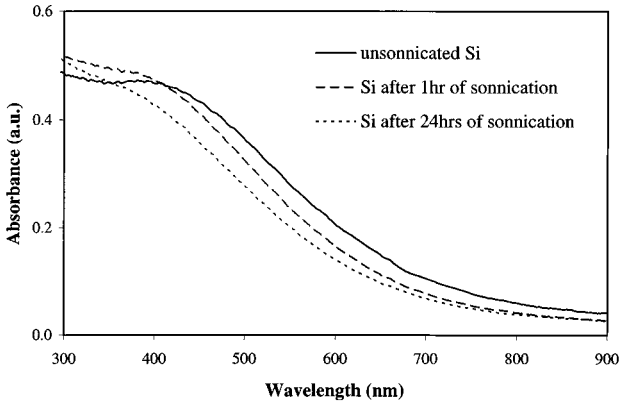

Figure 6. Effect of sonication on deagglomeration of Si nanoparticles in dilute suspension in ethanol.

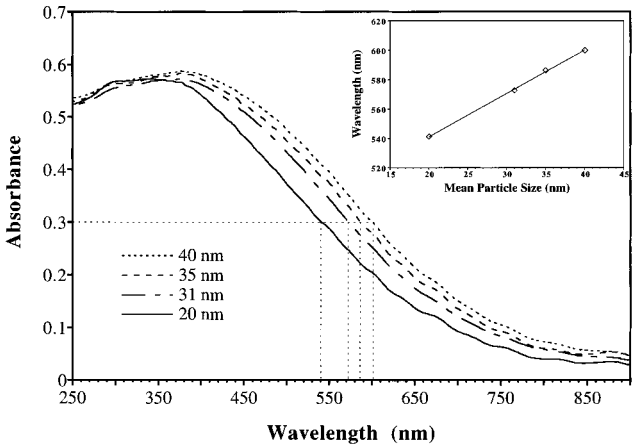

Figure 7. Nanosilicon UV−vis absorption as a function of particle size as determined by dynamic light scattering.

density (OD; ensuring similar amounts of Si tested) is in agreement with the above model, clearly indicating that the Si−O−Si absorbance increases proportionally with particle size. Future studies will be directed toward Raman spectroscopy and comparative dark/bright field electron microscopy in order to accurately quantify the ratio of silicon to silicon dioxide in these samples. In addition intensive research is presently underway to controllably oxidize, etch, and modify the surface of these nanoparticles.

Figure 5 illustrates the UV−vis spectra of the starting bulk Si powder, the as-milled Si powder, and the separated colloidal Si. The suspensions of the bulk and as-milled powders (both black in color) show essentially featureless spectra, with absorbance throughout the visible range. On the other hand, the centrifuged nanosilicon colloid exhibits a window of increased transparency in the red portion of the visible spectrum, which is responsible for its lightly opalescent bright orange appearance. The optical absorption of nanosized silicon has been the topic of intense investigations.[16,26,39,40,45] On the basis of these results, the present colloidal Si spectrum (2.7×10^{-4} M) is consistent with relatively large size (20−40 nm) nanosilicon.[16,40,45] A plot of the square root of the absorption as a function of absorption energy clearly indicates the indirect bandgap nature of these Si nanoparticles, and fails to reveal the direct transition which usually occurs at about 3.4 eV.[16,40,45] Although the size of these particles is in the region where Mie optical extinction could appear,[16,46] considerable departure from the ideal spherical, crystalline motif and polydispersity could be the reason this phenomenon is not observed.

The typical one-decade absorbance span (abs = 0.47 vs 0.041 at 400 and 900 nm, respectively) of the present colloid, compared to the two-decade absorbance span of the similar-sized simulated spectrum[16,46] and experimentally obtained spectra from smaller (3−8 nm) Si nanoparticles,[16,40,45] is attributed mainly to scattering as well as contribution from the increased absorbance of amorphous Si. Since scattering is proportional to the cube of particle size, the small fraction of agglomerates in the range between 100 and 150 nm, indicated from DLS, is responsible for nearly 95% of the scattering intensity. These agglomerates apart from scattering they also red-shift the optical absorption as indicated by Figure 6, where mild sonication is utilized to temporarily break them up. Unfortunately, these results could not be corroborated with DLS due to the fact that accurate particle-size measuring involves a minimum of 2 h data collection.

In an other set of experiments, colloidal Si with a range of different sizes was prepared. Figure 7 illustrates the UV−vis spectra of different particle-size Si colloids where their concentration was adjusted such that they result in comparable optical density between 300 and 350 nm. As described above, these colloids were prepared by the combination of (i) successive depletion of small particles by continuous centrifugation cycles and (ii) gradual increase of surface oxidation which promotes flotation of larger particles. The gradual spectral red shift with increasing particle size (see inset) could be caused by a number of reasons. Quantum confinement effects could be one of them, although highly questionable in this size range.[16,20,46,47] On the other hand, Mie scattering, EMA, local field effects, and concentration of surface and/or bulk defects are more likely candidates to explain such a shift.[48] The colloids of larger sized particles appear more reddish in color and also exhibit increasing scattering, making them less suitable for fabrication of high-refractive index nanocomposites of increased transparency.

(45) Brus, L. E.; Szajowski, P. F.; Wilson, W. L.; Harris, T. D.; Schuppler, S.; Cirtin, P. H. *J. Am. Chem. Soc.* **1995**, *117*, 2915
(46) Aspens, D. E.; Studna, A. A. *Phys. Rev. B* **1983**, *27*, 985.
(47) Guzelian, A. A.; Katari, J. E. B.; Kadavanich, A. V.; Banin, U.; Hamad, K.; Juban, E.; Alivisatos, A. P.; Wolters, R. H.; Arnold, C. C.; Heath, J. R. *J. Phys. Chem.* **1996**, *100*, 7212.
(48) Xie, Y. H.; Hybertsen, M. S.; Wilson, W. L.; Ipri, S. A.; Carver, G. E.; Brown, W. L.; Dons, E.; Weir, B. E.; Kortan, A. R.; Watson, G. P.; Liddle, A. J. *Phys. Rev. B.* **1994**, *49*, 5386.

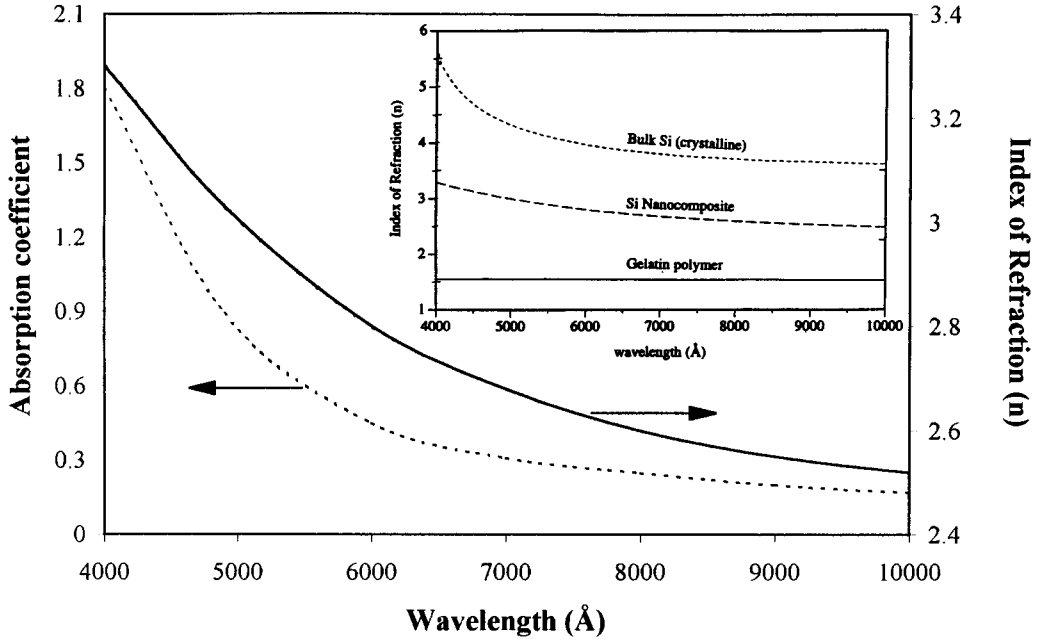

Figure 8. Index of refraction and absorption coefficient of a roughly 50/50 (w/w) gelatin/Si nanoparticles film prepared by spin coating. Insert compares the nanocomposite with bulk crystalline Si and gelatin, respectively.

High Refractive Index Nanocomposites. Gelatin and poly(ethylene oxide) have been extensively used for the fabrication of high refractive index nanocomposites with PbS.[18−20] The multiple functional sites in gelatin, a denatured protein, and its solubility in polar protic solvents such as water and ethanol makes it a matrix of choice for the fabrication of silicon-based nanocomposites. Mixing an aqueous solution of gelatin with the ethanolic suspension of Si nanoparticles and concentrating by bubbling N_2, a viscous brown liquid was obtained. The color of this liquid offers a first indication that gelatin strongly interacts with the silicon nanoparticles and prevents them from agglomerating which would otherwise have resulted in a black, non transparent liquid. Low-speed, slow acceleration spin coating results in high-quality films (ca. 30−50 nm) that are further densified by vacuum annealing at 150 °C.

Figure 8 illustrates the refractive index of ca. 50/50 (w/w) gelatin/Si nanocomposite determined by ellipsometry over the visible and near IR region. The refractive index (n) and absorption coefficient (k) were determined by numerically fitting a series of ellipsometric data over the entire wavelength (4000−10 000 Å) and angular (65−80°) range. On the basis of the low density and high refractive index of Si, these composites offer one of the lowest weight to refractive index ratio. The gradual decrease of refractive index with increasing wavelength is similar to that of bulk silicon, shown in inset of Figure 8. This is in excellent agreement to the theory[19,20] based on volume fraction which for the present nanocomposite is ca. 64/36 (v/v) gelatin/Si. The absorption coefficient of this film indicates the presence of suppressed absorption between 6000 and 10 000 Å. This is in good agreement with the absorption spectra of colloidal silicon, indicating that no further agglomeration has occurred in the solid composite film relative to that in the colloid suspension (see Figure 5). Scattering, as well as contributions from amorphous Si contribute to small absorption at higher wavelengths, suggesting that considerablly more effort has to be directed toward minimizing these effects. The intrinsic microstructure of this and similar nanocomposites will be addressed more extensively in a separate publication.

Conclusion

Silicon nanoparticles in the 20−40 nm range can be easily fabricated and subsequently isolated by mechanical attrition in large quantities. With the use of sonication−centrifugation cycles, particles with size distribution of about 25% can be isolated as indicated by transmission electron microscopy and dynamic light scattering results. These particles possess all the characteristics associated with their nanosized range and provide a useful starting material for producing high refractive index nanocomposites. Ellipsometric results indicate that the increase in the refractive index is proportional to the volume fraction of nanosized silicon. Suppressed absorption at longer wavelengths indicates the strong potential of such nanocomposites in applications where increased transparency in the red and near-IR part of the visible spectrum is essential.

Acknowledgment. The authors would like to thank Lamia Khairallah for helping with the TEM micrographs, Tom Fabian for assistance with ellipsometry measurements, and Prof. F. Jain for helpful discussions. Financial support from NSF Grant ECS 9528731 and the Critical Technologies Program through the Institute of Material Science, University of Connecticut are greatly appreciated.

CM970278Z